Efficient Generation of H_2 by Splitting Water with an Isothermal Redox Cycle

Christopher L. Muhich *et al.*

Science **341**, 540 (2013);
DOI: 10.1126/science.1239454

rotation axis is parallel to the observation direction. The high mode number of the OAM state, and the resulting rotational symmetry, means that the recorded frequency is higher than the rotation frequency itself by a factor of 2ℓ. A similar advantage in using OAM has been noted previously for fixed-angle measurement in both classical (*23*) and quantum (*24*) regimes. Of course, the maximum value of OAM mode that can be used is set by the modal bandwidth of the scattered light. However, increasing the bandwidth also reduces the fraction of the scattered light that falls within the scattered mode. Consequently, the degree of OAM enhancement of the rotation detection is a complicated function of the experimental conditions.

Although the Doppler shift, Doppler velocimetry, and their application to the remote measurement of transverse velocity are well known, our study recognizes that these phenomena have an angular equivalent. An analysis in terms of the OAM gives a clear and intuitive understanding of the angular case. This understanding indicates possible applications in multiple regimes. Two application areas of particular promise are the potential for the remote sensing of turbulence in backscattered light and the possible application to astronomy for the remote detection of rotating bodies.

References and Notes

1. L. Allen, M. W. Beijersbergen, R. J. C. Spreeuw, J. P. Woerdman, *Phys. Rev. A* **45**, 8185–8189 (1992).
2. A. M. Yao, M. J. Padgett, *Adv. Opt. Photon.* **3**, 161 (2011).
3. M. Harwit, *Astrophys. J.* **597**, 1266–1270 (2003).
4. L. Torner, J. P. Torres, S. Carrasco, *Opt. Express* **13**, 873–881 (2005).
5. S. Fürhapter, A. Jesacher, S. Bernet, M. Ritsch-Marte, *Opt. Express* **13**, 689–694 (2005).
6. F. Tamburini, B. Thidé, G. Molina-Terriza, G. Anzolin, *Nat. Phys.* **7**, 195–197 (2011).
7. G. A. Swartzlander Jr. *et al.*, *Opt. Express* **16**, 10200–10207 (2008).
8. B. A. Garetz, *J. Opt. Soc. Am.* **71**, 609 (1981).
9. I. Bialynicki-Birula, Z. Bialynicka-Birula, *Phys. Rev. Lett.* **78**, 2539–2542 (1997).
10. J. Courtial, K. Dholakia, D. A. Robertson, L. Allen, M. J. Padgett, *Phys. Rev. Lett.* **80**, 3217–3219 (1998).
11. S. Barreiro, J. W. Tabosa, H. Failache, A. Lezama, *Phys. Rev. Lett.* **97**, 113601 (2006).
12. L. Allen, M. Babiker, W. L. Power, *Opt. Commun.* **112**, 141–144 (1994).
13. A. Belmonte, J. P. Torres, *Opt. Lett.* **36**, 4437–4439 (2011).
14. J. Courtial, D. A. Robertson, K. Dholakia, L. Allen, M. J. Padgett, *Phys. Rev. Lett.* **81**, 4828–4830 (1998).
15. T. Asakura, N. Takai, *Appl. Phys.* **25**, 179–194 (1981).
16. R. Meynart, *Appl. Opt.* **22**, 535–540 (1983).
17. J. Leach, S. Keen, M. J. Padgett, C. D. Saunter, G. D. Love, *Opt. Express* **14**, 11919–11924 (2006).
18. S. Franke-Arnold *et al.*, *Opt. Express* **15**, 8619–8625 (2007).
19. J. Leach, M. R. Dennis, J. Courtial, M. J. Padgett, *N. J. Phys.* **7**, 55 (2005).
20. M. V. Vasnetsov, V. A. Pas'ko, M. S. Soskin, *N. J. Phys.* **7**, 46 (2005).
21. M. P. J. Lavery, G. C. G. Berkhout, J. Courtial, M. J. Padgett, *J. Opt.* **13**, 064006 (2011).
22. M. J. Padgett, *J. Opt. A* **6**, S263–S265 (2004).
23. S. M. Barnett, R. Zambrini, *J. Mod. Opt.* **53**, 613–625 (2006).
24. R. Fickler *et al.*, *Science* **338**, 640–643 (2012).

Acknowledgments: Supported by the UK Engineering and Physical Sciences Research Council and by the Defense Advanced Research Projects Agency InPho program through U.S. Army Research Office award W911NF-10-1-0395. S.M.B. and M.J.P. thank the Royal Society and Wolfson Foundation.

Supplementary Materials

www.sciencemag.org/cgi/content/full/341/6145/537/DC1
Materials and Methods
Figs. S1 and S2
Tables S1 and S2

1 May 2013; accepted 13 June 2013
10.1126/science.1239936

Efficient Generation of H_2 by Splitting Water with an Isothermal Redox Cycle

Christopher L. Muhich,[1] Brian W. Evanko,[1] Kayla C. Weston,[1] Paul Lichty,[1] Xinhua Liang,[1] Janna Martinek,[1] Charles B. Musgrave,[1,2]* Alan W. Weimer[1]*

Solar thermal water-splitting (STWS) cycles have long been recognized as a desirable means of generating hydrogen gas (H_2) from water and sunlight. Two-step, metal oxide–based STWS cycles generate H_2 by sequential high-temperature reduction and water reoxidation of a metal oxide. The temperature swings between reduction and oxidation steps long thought necessary for STWS have stifled STWS's overall efficiency because of thermal and time losses that occur during the frequent heating and cooling of the metal oxide. We show that these temperature swings are unnecessary and that isothermal water splitting (ITWS) at 1350°C using the "hercynite cycle" exhibits H_2 production capacity >3 and >12 times that of hercynite and ceria, respectively, per mass of active material when reduced at 1350°C and reoxidized at 1000°C.

Hydrogen is an attractive fuel because it produces only water when burned and can be used in highly efficient fuel cells (*1*, *2*), but it must be derived from some other chemical source, preferably a renewable one such as water (*3*). Splitting H_2O into H_2 and O_2 can be achieved by direct thermolysis (*4*–*6*)—for example, by solar thermal water splitting (STWS), which stores solar energy as H_2 at high theoretical maximum efficiencies (*7*, *8*). Unfortunately, direct thermolysis requires temperatures exceeding 2700°C that are impractical for industrial processes (*9*). However, two-step thermochemical H_2O splitting based on metal oxide reduction and oxidation (redox) cycles produces appreciable amounts of H_2 at the more technically feasible reduction temperatures T_{red} of 1200° to 1500°C (*4*, *10*).

In traditional two-step temperature-swing water splitting (TSWS), O_2 is generated by the reduction of a metal oxide during a high-temperature step according to

$$MO_x \rightarrow MO_{x-\delta} + \frac{\delta}{2}O_2 \qquad (1)$$

where $T_{red} \approx 1200°$ to 1500°C. The second step involves lowering the temperature and exposing the reduced metal oxide to water, which reoxidizes the metal oxide and produces H_2 according to

$$MO_{x-\delta} + \delta H_2O \rightarrow \delta H_2 + MO_x \qquad (2)$$

where oxidation temperature $T_{ox} < T_{red}$. One major advantage of this approach is that although the complete cycle produces H_2 and O_2 from H_2O,

Table 1. H2 production capacities and peak rates. A comparison of the solar thermal water splitting cycle capabilities is shown for both temperature swing and isothermal operation.

Operating temperature conditions (Red/Ox, °C)	Total H_2 generated (μmol g^{-1})	Peak H_2 generation rate (μmol g^{-1} s^{-1})
Hercynite 1350/1000	31.4 ± 2.3	0.06 ± 0.04
Hercynite 1500/1200	93.7 ± 19.2	0.32 ± 0.01
Hercynite 1350/1350	102 ± 18	0.55 ± 0.16
Ceria 1350/1000	16.4 ± 3.6	0.14 ± 0.04

[1]Department of Chemical and Biological Engineering, University of Colorado, Boulder, CO 80303, USA. [2]Department of Chemistry and Biochemistry, University of Colorado, Boulder, CO 80309, USA.

*Corresponding author. E-mail: alan.weimer@colorado.edu (A.W.W.); charles.musgrave@colorado.edu (C.B.M.)

they are produced in two separate steps, thus simplifying separation. Traditional thermodynamic analysis treats the process as a closed system and suggests that a substantial temperature difference between the oxidation and reduction steps is necessary to split water (*10*–*13*). However, large temperature swings between the reduction and oxidation steps cause thermodynamic inefficiencies from the irreversible heat losses incurred upon cooling of the active material to the oxidation temperature and the heat required solely to reheat the active material to its reduction temperature. Additionally, thermal stresses arising from the rapid thermal cycling of the system over large temperature differences present engineering and materials challenges in the design of high-temperature redox systems. However, contrary to widely accepted redox gas-splitting theory (*11*), we demonstrate that a change in temperature between reduction and oxidation steps is unnecessary, and that isothermal water splitting (ITWS) driven by swings in steam partial pressure not only produces H_2, but outperforms traditional TSWS and provides an opportunity for expanding renewable H_2 generation.

We used the "hercynite cycle" to examine TSWS and ITWS. Unlike more conventional nonvolatile metal oxide redox chemistries, in which reduction results in either O vacancy formation (e.g., cycles involving fluorite- or perovskite-type crystal structures such as CeO_2) (*14*) or the formation of solid solutions (e.g., ferrites) (*15*–*18*), reduction occurs via reaction between MFe_2O_4 and Al_2O_3 to form stable aluminates (*19*, *20*). During oxidation by H_2O, the M-ferrite spinel (MFe_2O_4) and alumina (Al_2O_3) reform, liberating H_2. For cobalt, the governing reactions are

$$CoFe_2O_4 + 3Al_2O_3 + \text{heat} \rightarrow CoAl_2O_4 + 2FeAl_2O_4 + \frac{1}{2}O_2 \quad (3)$$

$$CoAl_2O_4 + 2FeAl_2O_4 + H_2O \rightarrow CoFe_2O_4 + 3Al_2O_3 + H_2 \quad (4)$$

Reduction via reaction 3 begins at temperatures as low as 940°C, ~150°C below where ferrites and ceria start to reduce because the formation of the stable aluminates is more thermodynamically favorable than the formation of solid solutions or vacancies. Hence, the hercynite cycle is selected to demonstrate ITWS.

We used a hercynite cycle–active material composed of 19.8 weight percent $CoFe_2O_4$ on Al_2O_3 (*21*, *22*) in a stagnation flow reactor (*23*) to establish the baseline for comparison of TSWS to ITWS, as outlined in the supplementary materials and shown in fig. S1. In TSWS, the active materials are reduced (reaction 3) under inert gas flow (He) at 1350°C and 101.3 kPa for 60 min, then cooled to 1000°C for water reoxidation (reaction 4). A gas stream of 50 volume percent (vol%) steam in inert He was used to oxidize the reduced materials for 25 min, producing 31.4 ± 2.3 μmol of H_2 per gram of total material (Table 1). The extent of reduction and water-splitting capacity depends on the reduction temperature. Higher temperatures lead to a larger fraction of reduced Fe^{2+} ions. The number of available Fe^{2+} ions dictates the total H_2-generating capacity of the active material, with a maximum ratio of one H_2 molecule produced to every two Fe^{2+} cations. In our experiment, oxidation at 1000°C was characterized by a slow rate of reaction (a peak H_2 generation rate of 0.06 ± 0.04 μmol g^{-1} s^{-1}) and was likely surface reaction–limited (*20*). Because the oxidation reaction is slow, it is unlikely that most of the Fe^{2+} ions are reoxidized to Fe^{3+} during the 25 min, which limits the total H_2 production capacity of the 1350°/1000°C TSWS cycle.

Higher TSWS reduction and oxidation temperatures result in increased H_2 and O_2 production capacity and water-splitting rates. Active material cycled between 1500° and 1200°C produced 93.7 ± 19.2 μmol H_2 g^{-1} with a peak rate of 0.32 μmol H_2 g^{-1} s^{-1} (Table 1). The higher reduction temperature resulted in more complete reduction of the active material and a larger thermodynamic driving force for H_2O splitting. The higher rates of H_2 generation at 1500°/1200°C resulted from two factors: (i) the intrinsically higher reaction rates that arise from carrying out a kinetically limited process at a higher temperature, and (ii) the larger thermodynamic driving force for oxidation, which comes from the larger extent of reduction. The ability to perform water oxidation at temperatures above the onset of reduction suggests that ITWS is possible (*24*) and that the current

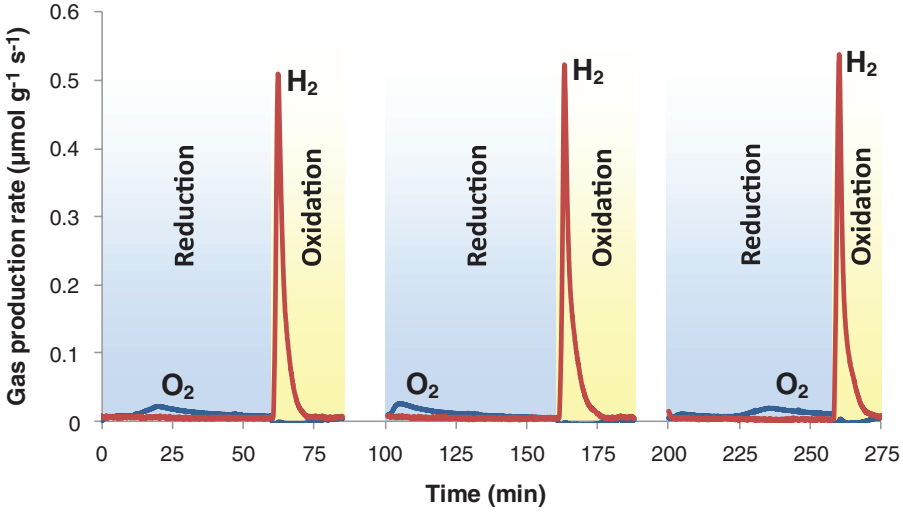

Fig. 1. Isothermal water splitting at 1350°C. The H_2 and O_2 generation rates are shown in red and blue, respectively.

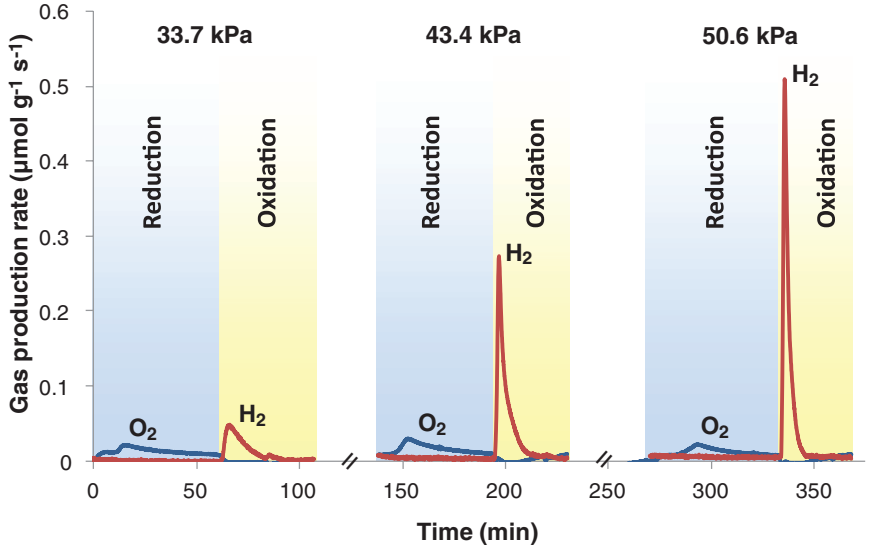

Fig. 2. The effect of steam pressure on 1350°C ITWS. From left to right: H_2O partial pressures of 33.7 kPa, 43.4 kPa, and 50.6 kPa.

understanding of the thermodynamics of STWS is incomplete.

Hercynite cycle–active materials split water in a two-step isothermal redox cycle, as exemplified by the 1350°C ITWS results shown in Fig. 1. H_2 generation under ITWS conditions was achieved at a temperature above the minimum reduction temperature by first flowing an inert gas through the reactor to sweep away O_2 generated during the reduction step and subsequently injecting steam during the oxidation step to produce H_2 (fig. S3). For 1350°C ITWS, the active particles produced 45.1 ± 7.6 μmol O_2 g^{-1} during 1 hour of reduction and 102 ± 18 μmol H_2 g^{-1} during 25 min of exposure to 50 vol% steam in He. During reduction, the initial O_2 plateaus arise from incomplete H_2O removal from the system. Once all steam is swept from the reactor, the O_2 peak occurs as the materials reduce, followed by the normal exponential decay as the reaction goes to completion. 1350°C ITWS produces substantially more O_2 and H_2 than 1350°/1000°C TSWS and slightly more O_2 and H_2 than 1500°/1200°C TSWS. The slight deviation of the 2.26:1 H_2/O_2 ratio from the expected 2:1 ratio, although within error, likely arises from slight differences in the sensitivities and response times of the O_2 analyzer and of the mass spectrometer used for measuring H_2. The higher gas-splitting production capacity of ITWS was accompanied by a higher H_2 production rate of 0.55 ± 0.16 μmol H_2 g^{-1} s^{-1}. ITWS's higher rate of H_2 generation and its lack of irreversible heat losses associated with the change in temperature between oxidation and reduction steps (which is required for TSWS) results in ITWS having a higher theoretical efficiency than TSWS, with the conditions examined in this study (see the supplementary materials for a comparison of ITWS and TSWS efficiencies, in particular table S1).

Traditional TSWS thermodynamic theory uses a closed-system model in which an oxidation temperature lower than the reduction temperature raises the chemical potential of the oxidizing gas and reduced metal oxide above that of the product gases and oxidized material in order to drive the oxidation reaction. In contrast, ITWS in an open system uses swings in the partial pressure of the oxidizing gas to produce the chemical potential differences that drive the oxidation and reduction steps. To form a two-step water-splitting closed-cycle system, a process for the recombination of H_2 and O_2 must be included, such as an electrolyzer (fig. S4) (*5*). In the ITWS process, the partial pressure of generated gaseous reduction and oxidation products remains low by sweeping them from the reactor. The low chemical potential of O_2 during reduction and high H_2O and low H_2 chemical potentials during oxidation drive the respective reactions forward to enable ITWS. Furthermore, sweeping the product gases away from the metal oxide prevents reverse reactions from occurring.

Not only are redox reactors open systems, but the reactions take place between gases adsorbed on the surface and the solid phase. Thus, the chemical potential and the coverage of gas molecules adsorbed on the surface are the relevant quantities to consider for analyzing redox reaction thermodynamics. Because the coverage of adsorbates, and therefore their chemical potentials, are related to partial pressure, the oxidation reaction is driven by increasing the H_2O partial pressure and maintaining a low H_2 partial pressure. Therefore, ITWS relies on a chemical potential difference derived from readily adjustable gas-phase partial pressures, rather than having to depend on the problematic large temperature changes of TSWS.

This analysis suggests that by increasing the partial pressure of the oxidizing gas, we can drive the water-splitting reaction further toward the products. Indeed, an increased partial pressure of water resulted in higher H_2 production capacities at higher rates (Fig. 2). For 1350°C ITWS, steam concentrations in He of 33%, 43%, and 50% (overall pressure held at 101.3 kPa) correspond to H_2 production capacities of 40 ± 9, 72 ± 8, and 102 ± 18 μmol H_2 g^{-1} and peak production rates of 0.06 ± 0.02, 0.15 ± 0.07, and 0.55 ± 0.16 μmol H_2 g^{-1} s^{-1}, respectively. The increased peak production rates correspond to shorter oxidation times, as expected. The higher steam pressure results in a higher water chemical potential on the active material's surface, which provides a higher thermodynamic driving force for oxidation. Additionally, the higher steam concentrations increase the overall rate of reaction by increasing the reactant concentration. This result suggests that decreases in the time required for the oxidation step and possible increases in the ITWS temperature can be achieved by increasing the partial pressure of the oxidizing gas. Furthermore, relative to the 1350°/1000°C ceria redox cycle (which is considered the current state-of-the-art material for TSWS redox processing), the ITWS hercynite cycle produces >6 times as much H_2 on a total-mass basis and >12 times as much H_2 on an active-materials basis (47% active) (Fig. 3 and Table 1). In addition to ITWS's favorable kinetics and thermodynamics (Fig. 3 and table S1), ITWS reduces both irreversible heat losses and thermal shock concerns that limit the efficiency and operations of traditional TSWS.

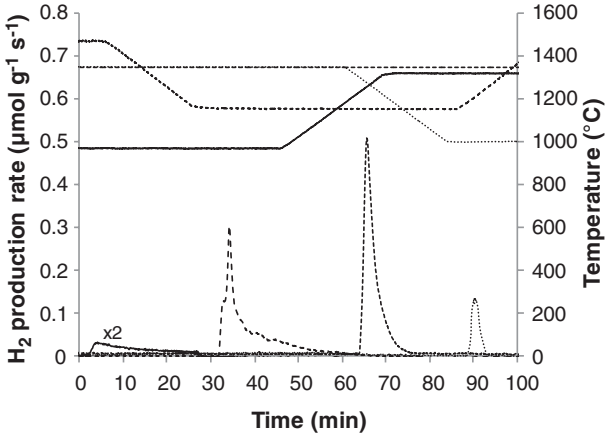

Fig. 3. A comparison of STWS. H_2 production curves are shown for hercynite cycle–based 1350°/1000°C TSWS (solid line, shown at twice its experimentally found value), 1500°/1200°C TSWS (long dashed line), 1350°C ITWS (short dashed line), and ceria-based 1350°/1000°C TSWS (dotted line).

References and Notes

1. L. Barreto, A. Makihira, K. Riahi, *Int. J. Hydrogen Energy* **28**, 267–284 (2003).
2. J. M. Ogden, *Annu. Rev. Energy Environ.* **24**, 227–279 (1999).
3. N. S. Lewis, D. G. Nocera, *Proc. Natl. Acad. Sci. U.S.A.* **103**, 15729–15735 (2006).
4. T. Nakamura, *Sol. Energy* **19**, 467–475 (1977).
5. E. A. Fletcher, R. L. Moen, *Science* **197**, 1050–1056 (1977).
6. Z. Wang, R. R. Roberts, G. F. Naterer, K. S. Gabriel, *Int. J. Hydrogen Energy* **37**, 16287–16301 (2012).
7. A. Steinfeld, *Sol. Energy* **78**, 603–615 (2005).
8. E. A. Fletcher, *J. Sol. Energy Eng. Trans. ASME* **123**, 63 (2001).
9. C. Perkins, A. W. Weimer, *Int. J. Hydrogen Energy* **29**, 1587–1599 (2004).
10. C. Perkins, A. W. Weimer, *AIChE J.* **55**, 286–293 (2009).
11. B. Meredig, C. Wolverton, *Phys. Rev. B* **80**, 245119 (2009).
12. T. Kodama, *Prog. Energy Combust. Sci.* **29**, 567–597 (2003).
13. A. Steinfeld, S. Sanders, R. Palumbo, *Sol. Energy* **65**, 43–53 (1999).
14. W. C. Chueh *et al.*, *Science* **330**, 1797–1801 (2010).
15. M. D. Allendorf, R. B. Diver, N. P. Siegel, J. E. Miller, *Energy Fuels* **22**, 4115–4124 (2008).
16. T. Kodama, N. Gokon, R. Yamamoto, *Sol. Energy* **82**, 73–79 (2008).
17. T. Kodama, Y. Kondoh, R. Yamamoto, H. Andou, N. Satou, *Sol. Energy* **78**, 623–631 (2005).
18. Y. Tamaura, A. Steinfeld, P. Kuhn, K. Ehrensberger, *Energy* **20**, 325–330 (1995).
19. J. R. Scheffe, J. H. Li, A. W. Weimer, *Int. J. Hydrogen Energy* **35**, 3333–3340 (2010).
20. D. Arifin, V. J. Aston, X. H. Liang, A. H. McDaniel, A. W. Weimer, *Energy Environ. Sci.* **5**, 9438 (2012).
21. X. Liang, N.-H. Li, A. W. Weimer, *Microporous Mesoporous Mater.* **149**, 106–110 (2012).
22. P. Lichty *et al.*, *Int. J. Hydrogen Energy* **37**, 16888–16894 (2012).
23. J. R. Scheffe *et al.*, *Chem. Mater.* **23**, 2030–2038 (2011).
24. J. R. Scheffe, A. H. McDaniel, M. D. Allendorf, A. W. Weimer, *Energy Environ. Sci.* **6**, 963 (2013).

Acknowledgments: Supported by NSF grant CBET 0966201 and by the U.S. Department of Energy Fuel Cell Technologies Office through the Solar Thermochemical Hydrogen (STCH) directive. We thank V. Aston, A. Sagastegui, and C. Herradón. Data used in this study will be made freely available upon request.

Supplementary Materials

www.sciencemag.org/cgi/content/full/341/6145/540/DC1
Materials and Methods
Supplementary Text
Figs. S1 to S4
Table S1
Reference (*25*)

22 April 2013; accepted 2 July 2013
10.1126/science.1239454